

Nanoscale

Accepted Manuscript



This is an *Accepted Manuscript*, which has been through the Royal Society of Chemistry peer review process and has been accepted for publication.

Accepted Manuscripts are published online shortly after acceptance, before technical editing, formatting and proof reading. Using this free service, authors can make their results available to the community, in citable form, before we publish the edited article. We will replace this *Accepted Manuscript* with the edited and formatted *Advance Article* as soon as it is available.

You can find more information about *Accepted Manuscripts* in the [Information for Authors](#).

Please note that technical editing may introduce minor changes to the text and/or graphics, which may alter content. The journal's standard [Terms & Conditions](#) and the [Ethical guidelines](#) still apply. In no event shall the Royal Society of Chemistry be held responsible for any errors or omissions in this *Accepted Manuscript* or any consequences arising from the use of any information it contains.

Nonradiative Energy Transfer in Colloidal CdSe Nanoplatelet Films

*Burak Guzelturk^{1,3}, Murat Olutas^{1,2}, Savas Delikanli¹, Yusuf Kelestemur¹, Onur Erdem¹ and
Hilmi Volkan Demir^{1,3,*}*

¹ Department of Electrical and Electronics Engineering, Department of Physics, UNAM -
Institute of Materials Science and Nanotechnology, Bilkent University, Ankara 06800 Turkey

² Department of Physics, Abant Izzet Baysal University, Bolu 14280, Turkey

³ *Luminous!* Center of Excellence for Semiconductor Lighting and Displays, School of Electrical
and Electronic Engineering, School of Physical and Mathematical Sciences, Nanyang
Technological University, Nanyang Avenue, Singapore 639798, Singapore

*Corresponding Author:

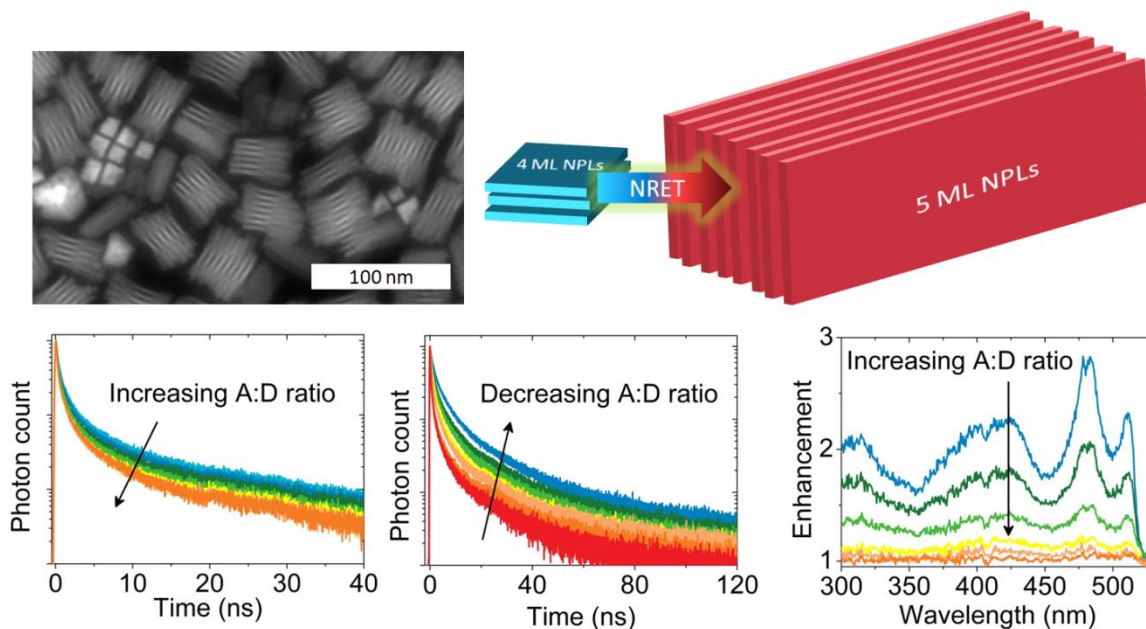
Email: volkan@bilkent.edu.tr, hvdemir@ntu.edu.sg

Phone.: +90 312 290-1021

Fax: +90 312 290-1123

Abstract

Nonradiative energy transfer (NRET) has been extensively studied in assemblies of colloidal nanocrystals (quantum dots) and nanorods (quantum wires). In this work, we present the first account of spectroscopic evidence of NRET in solid thin films of CdSe based colloidal nanoplatelets (NPLs), also known as colloidal quantum wells. NRET is investigated as a function of the concentration of two NPL populations having different vertical thicknesses via steady state and time resolved spectroscopy. NRET takes place from the NPLs having a smaller vertical thickness (i.e., larger bandgap) to the ones having a larger vertical thickness (i.e., smaller bandgap) with efficiency up to ~60%. Here, we reveal that the NRET efficiency is limited in these NPL solid film assemblies due to the self-stacking of NPLs within their own population causing increased distance between donor-acceptor pairs, which is significantly different than previously studied colloidal quantum dot based architectures for nonradiative energy transfer.



KEYWORDS: Colloidal quantum wells, colloidal nanoplatelets, nonradiative energy transfer, Förster resonance energy transfer, time resolved fluorescence spectroscopy.

Introduction

Colloidal semiconductor nanoplatelets (NPL), which have strong quantum confinement only in one dimension (1D), have been recently synthesized in the form of CdE (E= Se, S and Te) with precisely controlled vertical thicknesses.^{1,2} These NPLs exhibit unique and favorable optical properties including narrow photoluminescence spectra due to the absence of inhomogeneous broadening, splitting of the electron/light-hole and electron/heavy-hole transitions, and giant oscillatory strength resembling their epitaxial counterparts.²⁻⁶ These features differentiate the NPLs from other colloidal semiconductor nanomaterials having different quantum confinement dimensionality such as 3D-confined colloidal nanocrystals (quantum dots) and 2D-confined nanorods (quantum wires). Furthermore, these advantageous properties make the NPLs extremely promising for optoelectronic applications including LEDs⁷ and lasers⁸. To date, CdSe NPLs having zinc blende crystal structure have been the most extensively studied type among other types of NPLs thanks to their optimized synthesis route resulting in high quality NPLs having a magic sized vertical thickness with reasonably uniform lateral size distribution.^{2,9} The vertical thickness of the NPLs is denoted by the number of monolayers (MLs) of the repeating lattice units. Commonly synthesized vertical thickness of the CdSe NPLs ranges from 3 to 6 MLs. The peak emission wavelength of 3, 4 and 5 ML CdSe NPLs corresponds to 463, 513 and 551 nm, respectively, with emission full-width at half-maxima (FWHM) as narrow as 8 nm at room temperature.

Previously optical properties of the NPLs have been studied both in solution and solid phases. In the case of solid thin films, either ensemble or single NPL based studies have been reported.^{4-6,10-13} However, in all of these previous reports only a single population of NPL emitter having a fixed vertical thickness was considered and investigated. On the other hand, it is widely known that nonradiative energy transfer (NRET), also commonly referred to as Förster resonance energy transfer (FRET)¹⁴, can take place within the close-packed assemblies of semiconductor nanostructures (e.g., colloidal nanocrystals and nanorods) with different sizes through near field dipole-dipole coupling.¹⁵⁻¹⁸ Therefore, it is expected to realize NRET in close-packed solid films incorporating NPL populations, each of a different vertical thickness. However, NRET has not been systematically studied nor demonstrated in the solid assemblies of the NPLs to date. In this work, we show the first spectroscopic evidence of NRET within the solid films of CdSe NPLs of vertical thicknesses 4 and 5 ML. We systematically investigate NRET as a function of the donor-to-acceptor ratio via time resolved and steady state fluorescence spectroscopy, which conclusively reveals the existence of NRET from 4 to 5 ML NPLs. Furthermore, the NRET efficiency is analyzed and it is found out that it is limited to ~60%. This limitation is understood by investigation of the morphology of the mixed solid thin films, where stacking of the donor and acceptor NPLs within their own population results in to a nanoscale phase segregation between the donor-acceptor pairs of NPLs. This type of phase segregation has not been observed in the mixed donor-acceptor pairs of the colloidal quantum dots and rods.

Results and Discussion

CdSe NPLs with 4 and 5 ML vertical thicknesses exhibiting 30-50% photoluminescence quantum yield were synthesized using a modified recipe and dissolved in hexane (see the

Experimental Section).¹ The absorption (dashed) and photoluminescence (solid) spectra of the synthesized 4 and 5 ML NPLs are shown in Figure 1. Absorbance of the NPLs exhibits pronounced sharp features corresponding to the electron/light-hole (480 nm for 4 ML and 518 nm for 5 ML) and the electron/heavy-hole (512 nm for 4 ML and 549 nm for 5 ML) transitions characteristic to the NPLs.² During the synthesis of 4 and 5 ML NPLs, quantum dots and/or NPLs with different vertical thickness could be also possibly synthesized as a side product. However, using size selective precipitation via ultracentrifugation it is possible to totally eliminate these side products. As shown by the absorbance of the NPL solutions after size selective precipitation in Figure 1, there is no contribution from the side products. Therefore, we were able to achieve NPL solutions containing only single NPL population. In these NPLs, radiative recombination takes place at the electron/heavy-hole transition resulting in the peak emission wavelength at 513 nm from 4 ML NPLs and 551 nm from 5 ML NPLs, both with FWHM of ~8 nm as shown by Figure 1.

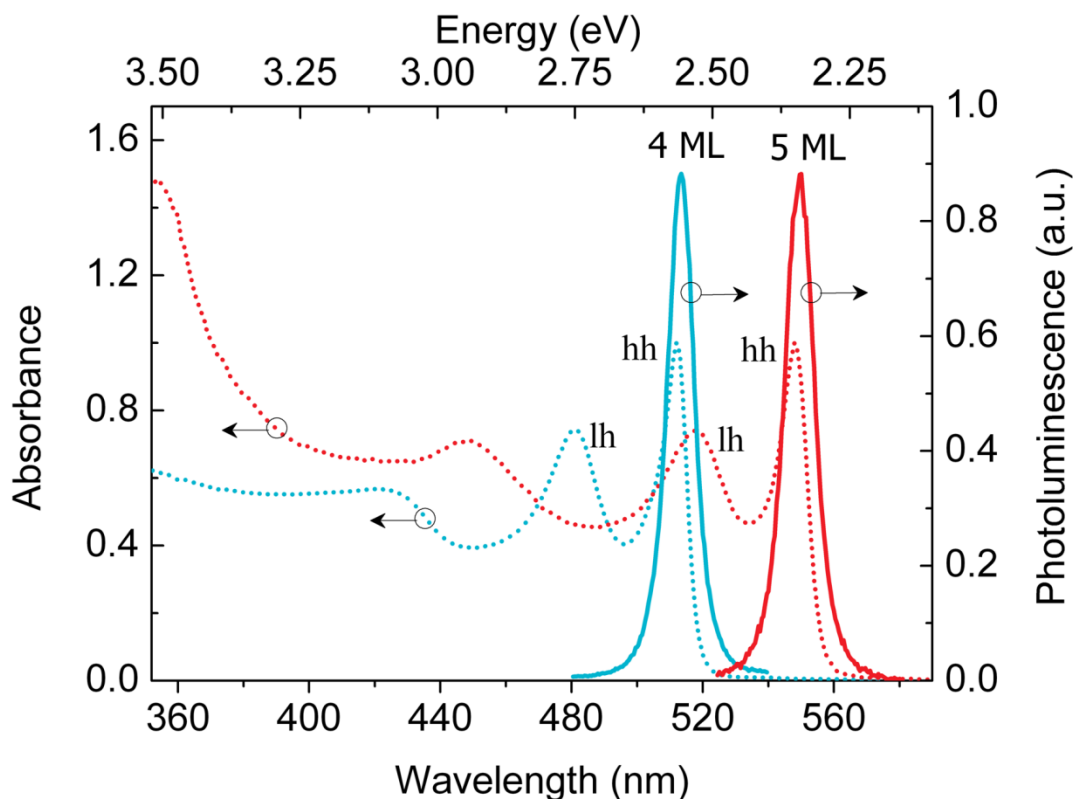


Figure 1. Absorption (dashed lines) and photoluminescence (solid lines) of the 4 ML (cyan) and 5 ML (red) NPLs.

High-angle annular dark field transmission electron microscopy (HAADF-TEM) was utilized to image the 4 and 5 ML NPLs on carbon coated ultrathin copper grids as shown in Figure 2a and 2b, respectively. The average size of the 4 ML NPLs is 23.57 nm (± 2.90 nm) by 12.17 nm (± 1.94 nm), and that of 5 ML NPLs is 26.32 nm (± 2.55 nm) by 9.04 nm (± 1.41 nm). Both NPLs were observed to form stacks on TEM grids, as can be observed in Figure 2, which that has been previously demonstrated in the literature.^{11,19} Stacking of the NPLs can be intentionally triggered via addition of polar solvents such as ethanol into the apolar solvents of the NPLs, or it can also be favored during the solid film formation. Bending of the NPLs is not expected to alter its excitonic properties owing to the strong quasi-one-dimensional quantum confinement and mechanical flexibility of the NPLs.¹¹

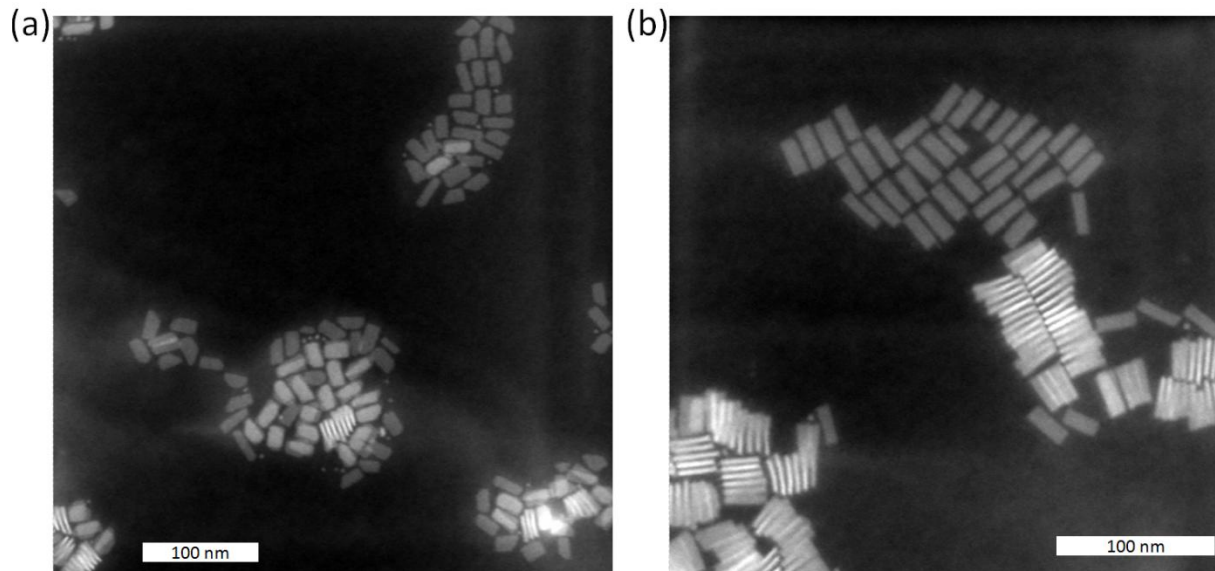


Figure 2. HAADF-TEM images of the NPLs of (a) 4 ML having the average size of 23.57 nm (\pm 2.90 nm) by 12.17 nm (\pm 1.94 nm) and (b) 5 ML having the average size of 26.32 nm (\pm 2.55 nm) by 9.04 nm (\pm 1.41 nm). Stacking of the NPLs is clearly visible in both NPL populations. The scale bars are 100 nm.

NPLs were transferred to solid thin films via spin-coating them on pre-cleaned quartz substrates. The surface coverage and homogeneity of the mixed NPL thin film samples were inspected via confocal microscopy using pump laser as Ar-ion laser line at 458 nm, which can pump both of the NPL populations simultaneously. Figure 3 presents exemplary case of mixed thin film sample having acceptor-to-donor molar ratio of 0.28. Figure 3a shows the confocal image of the sample when the collection channel is located in the spectral range of 505-530 nm matching only the emission of 4 ML NPLs. Figure 3b shows the confocal image of the same location of the same sample when the collection channel is located in the spectral range of 560-615 nm matching only the emission of 5 ML NPLs. Both confocal images indicate very high surface coverage and film uniformity owing to the observation of homogenous emission all around the sample surface except a few brighter spots indicating aggregation. Therefore, the spin-coated samples are highly homogenous at the microscale. However, as we will discuss

further, we observe stacking of the NPLs via TEM imaging leading to a nanoscale phase separation between the 4 and 5 ML NPLs.

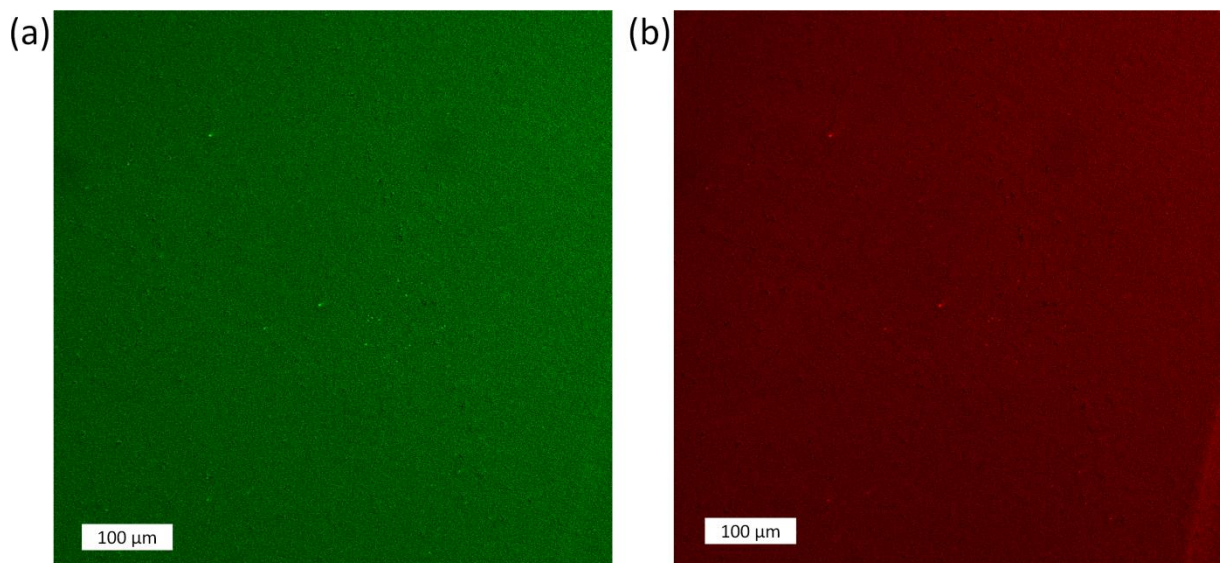


Figure 3. Confocal images of the mixed solid films of the 4 and 5 ML NPLs. The collection window is (a) 505-530 nm matching only the emission of 4 ML NPLs, (b) 560-615 nm matching only with the emission of 5 ML NPLs. In both images, artificial coloring is used to represent the emission intensity. The scale bar is 100 μm .

For the NRET study, we prepared eight solid thin film samples. Two of these were the only donor and only acceptor reference samples and rest of them were the mixed samples having different acceptor-to-donor (A:D) molar ratios. We then performed time resolved fluorescence spectroscopy on these samples as shown by the fluorescence decay curves in Figure 4. Figure 4a and 4b depict the fluorescence decay curves of the 4 and 5 ML NPLs, respectively, for different samples with varying A:D ratio, which is calculated by using Beer-Lambert law. The concentration of the donor and acceptor NPLs is calculated to be 7.976×10^{-7} and 4.493×10^{-8} M using the absorption cross sections (at 3.1 eV) of 3.1×10^{-14} and 2.5×10^{-13} cm^2 , respectively.^{10,20} In Figure 4a, as the A:D ratio is increased, the donor NPLs are observed to decay faster. This indicates a new decay channel, of energy transfer, being opened up for the donor NPLs as the

density of the acceptor NPLs is increased. In the case of decay kinetics of the acceptor 5 ML NPLs, we observe that the fluorescence decay is slowed down compared to the decay of the only acceptor solid film. As frequently observed for the colloidal quantum dot based acceptors, elongation of the fluorescence decay indicates the presence of exciton feeding via NRET into acceptor material.²¹ Rise component of the fluorescence decay in the acceptor NPLs do not significantly change upon mixing with donor NPLs since acceptor NPLs are on their own strongly excited via absorption of the pulsed pump laser at 375 nm.

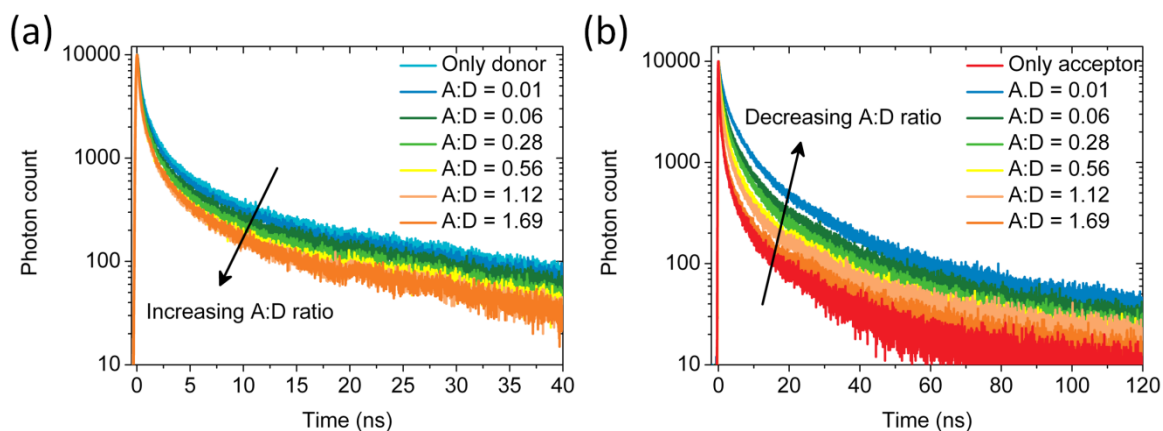


Figure 4. Time resolved fluorescence spectroscopy of the (a) 4 ML and (b) 5 ML NPLs in their solid thin films.

The fluorescence decay of the NPLs exhibit multi-exponential decay behavior as attributed to the complex decay kinetics of these materials.¹⁰ Generally, three or four exponential decay functions were employed in the literature to fit the fluorescence decay of the NPLs. In this work, we employ four exponential decay functions and fit the fluorescence decay curves in Figure 4 with near unity reduced χ^2 and uniform residuals (see Table S1 and S2 for the fluorescence lifetime components and their fractional contributions). A possible approach to handle multi-exponential decay kinetics is to use amplitude averaged fluorescence lifetimes, although this does not fully capture the individual decay kinetics. Previously, amplitude averaged fluorescence

lifetimes were also employed to investigate the NRET kinetics in the case of donors having intrinsic multi-exponential decay channels.²² Therefore, for the further analysis of the NRET rates and efficiencies, we employ the amplitude averaged fluorescence lifetimes as presented in Table 1. As shown in Table S1 and S2, all of the fluorescence decay components are altered due to NRET. This suggests that all of the complex fluorescence decay channels are affected due to the presence of nonradiative energy transfer. As the A:D ratio is increased from 0.01 to 1.69 (Figure 4a), we observe that the donor fluorescence decay curves become progressively faster (i.e., the fluorescence lifetime of the donor NPLs shortens). This can be explained with the increase in number of the acceptor NPLs per donor NPL. It is also important to note that for the A:D ratios above 0.56, we observe that the donor decay curves do not change noticeably. This indicates a saturation of NRET process between these donor-acceptor pairs. In the case of acceptor decays in Figure 4b, the acceptor lifetime is elongated as high as by 6-folds (see Table 1) in the case of small A:D ratios, where there are a large number of donor NPLs per acceptor NPL. As the A:D ratio is increased, the acceptor decays converge to the decay of the only acceptor thin film since the number of donors per acceptor is considerably decreased. Therefore, most of the acceptors are excited directly via pump laser without NRET, although all of the available donor NPLs, which are less in number, are transferring at a maximum rate. This shows that, from the acceptor point of view, exciton feeding becomes insignificant at high A:D ratios. As shown in Table 1, NRET rates are also calculated for different A:D ratios, where the predicted NRET rate can be as high as 1.193 ns^{-1} .

Table 1. Amplitude averaged fluorescence lifetimes of the donor and acceptor NPLs for the samples having varying A:D ratio. Predicted NRET rates (ns^{-1}) are also presented.

Acceptor – Donor Ratio (A:D)						
Only donor (or acceptor)	0.01	0.06	0.28	0.56	1.12	1.69

τ_{donor} (ns)	1.18	1.02	0.84	0.78	0.57	0.49	0.54
τ_{acceptor} (ns)	0.66	4.13	2.59	2.15	1.79	1.47	0.83
NRET Rate (ns ⁻¹)	-	0.133	0.343	0.435	0.907	1.193	1.00

Additionally, we employed photoluminescence excitation (PLE) spectroscopy to investigate the steady state evidence of NRET in these mixed NPL solid thin films. We measured the PLE spectra of the only donor and only acceptor thin film samples while monitoring the peak emission wavelength of the 4 and 5 ML NPLs, respectively, as shown in Figure 5a. These PLE spectra highly resemble absorption spectra of these NPLs (see Figure 1). Spectral features observed at 480 and 518 nm correspond to the electron/light-hole transitions in 4 and 5 ML NPLs, respectively. Figure 5b shows the evolution of the PLE curves measured at the peak emission wavelength of the acceptor (5 ML NPLs), as the A:D ratio in the mixed samples is changed from 0.01 to 1.69, together with the PLE of the only acceptor sample. Here, we normalize the PLE curves at 530 nm, since there is no contribution from the donor NPLs at this wavelength (i.e., neither absorption nor neither emission). In Figure 5b, at small A:D ratios, where there are a large number of donors per acceptor, we observe emerging spectral features in the PLE spectrum of the acceptor emission, which is attributed to the NRET from the donor NPLs.

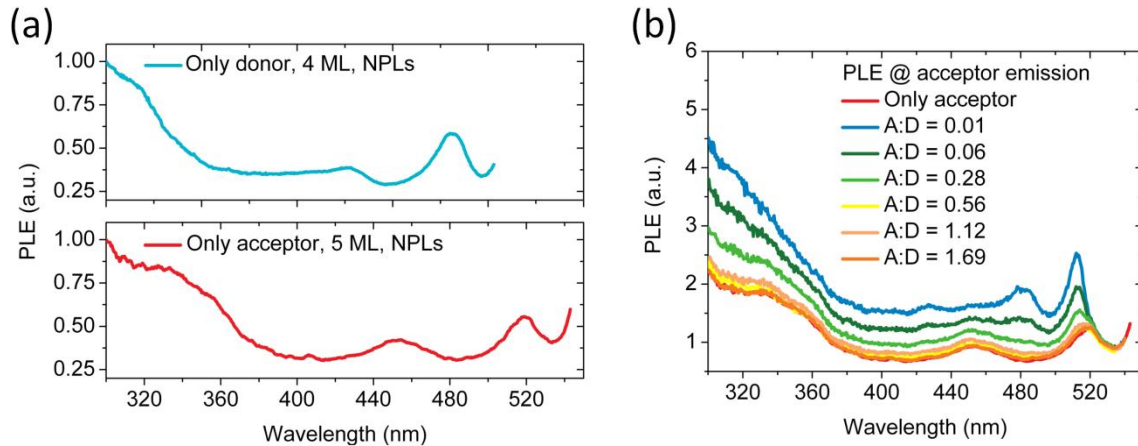


Figure 5. (a) Photoluminescence excitation spectra of the 4 and 5 ML NPLs featuring the electron/light-hole and continuum bands. (b) Enhancement of the 5 ML NPL PLE owing to the NRET from the 4 ML NPLs.

To understand the origin of the newly emerged spectral features in Figure 5b, we calculated the spectral enhancement of the PLE curves in the mixed samples normalizing with respect to the only acceptor sample. The resulting curves are presented in Figure 6. We observe that the spectral enhancement resembles the PLE spectra of the donor NPLs. The features observed around 510 and 480 nm correspond to the electron/heavy-hole and electron/light-hole transitions in the donor 4 ML NPLs. This indicates that across spectral ranges where the donor NPLs are better excited, the energy transfer into the acceptor NPLs becomes stronger and more efficient. In addition, at the higher photon energy tail of 480 nm peak, there is enhancement of the PLE due to the continuum absorption states in the donor NPLs. The largest enhancement of the PLE of the acceptor NPLs is achieved when the donors are 100 \times of the acceptors (corresponding to the A:D ratio of 0.01) due to presence of abundant donor NPLs increasing the probability of the funneling excitons into the acceptor NPLs. At small A:D ratios, the dominant excitation mechanism of the acceptor NPLs is through NRET since PLE enhancement factor as high as 2.8-folds could be achieved. As the A:D ratio is increased, we observe that enhancement of the PLE gradually diminishes since the number of donors per acceptor is concomitantly

decreased. At these large A:D ratios, the acceptor NPLs are dominantly excited via the pump light instead of being excitonically pumped by NRET from the donor NPLs since the PLE enhancement factor is close to 1 in this range.

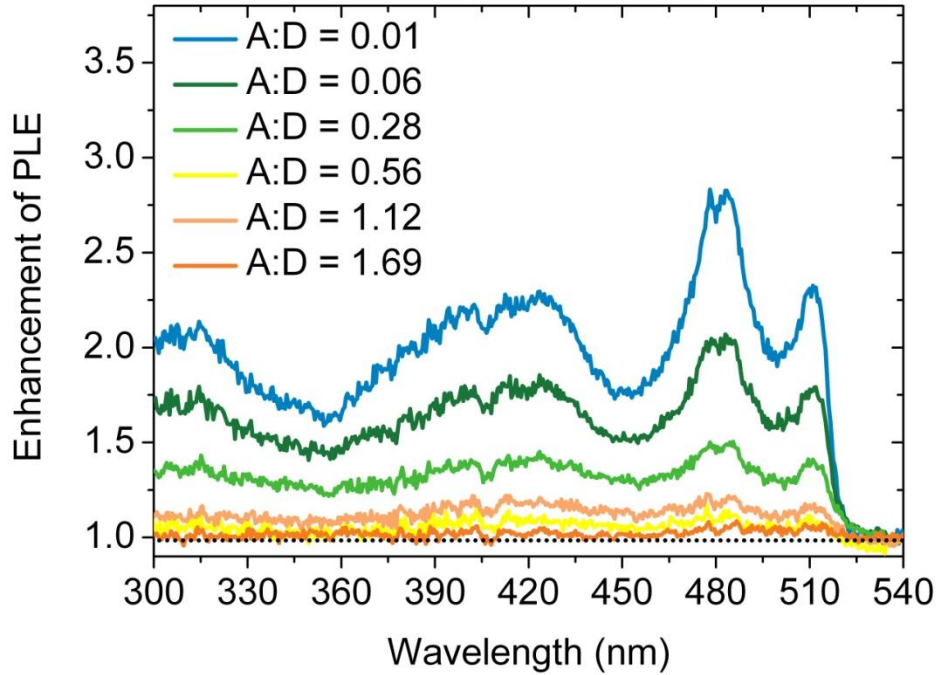


Figure 6. Enhancement of the acceptor NPL emission excitation exhibiting spectral features resembling the spectral PLE features of the donor NPLs. At small A:D ratios, the dominant excitation mechanism of the acceptor NPLs is through NRET, whereas at large A:D ratios the acceptor NPLs are dominantly excited through direct absorption of the pump photons.

Figure 7 shows the NRET efficiency as a function of the A:D ratio as computed as follows.

$$\gamma_{donor} = \gamma_{radiative} + \gamma_{nonradiative} \quad (1)$$

$$\gamma_{donor_with_acceptor} = \gamma_{radiative} + \gamma_{nonradiative} + \gamma_{NRET} \quad (2)$$

$$\eta_{NRET} = 1 - \frac{\tau_{donor_with_acceptor}}{\tau_{donor}} \quad (3)$$

Here, γ_{donor} ($= \frac{1}{\tau_{donor}}$) is the fluorescence decay rate of the donor NPLs in the absence of acceptors. $\gamma_{radiative}$ and $\gamma_{nonradiative}$ are the intrinsic radiative and nonradiative decay rates of the donor NPLs, respectively. $\gamma_{donor_with_acceptor}$ ($= \frac{1}{\tau_{donor_with_acceptor}}$) is the fluorescence decay rate of the donor NPLs in the presence of acceptors. γ_{NRET} is the rate of the NRET process and η_{NRET} is the efficiency of the NRET. Because of the architecture and dimensionality of the NPLs, the NRET efficiency is expected to be large since the close-packing in NPL assemblies would be achieved owing to the small magic sized vertical thickness (3 ML ~0.9 nm, 4 ML ~1.2 nm, 5 ML ~1.5 nm) of the NPLs. In this work, however, NRET efficiencies are observed to be limited to 60% as given in Figure 7. Based on Coulombic dipole-dipole coupling, we compute the Förster radius²² to be 10.83 nm between the donor-acceptor pairs using the following parameters. The extinction coefficient of 5 ML NPLs at 500 nm is calculated as $4.86 \times 10^7 \text{ M}^{-1} \text{ cm}^{-1}$, the quantum yield of the donor NPLs as 10%, the dipole orientation factor (κ^2) as 2/3 assuming random transition dipole orientations and the refractive index of the medium as 1.8. If the 4 and 5 ML NPLs were to perfectly assemble in the form of inter-mixed stacks (similar to two bunches of poker cards well mixed together), then the donor-to-acceptor separation distance would be expected to be comparable to 4-5 nm on the average due to interpenetrating ligands as previously demonstrated by small-angle x-ray scattering measurements (SAXS).^{11,19} Therefore, NRET greater than 95% would have been possible in these solid films in the case of perfect inter-stacking. On the other hand, we experimentally observe the saturation of the NRET efficiencies below such high efficiency level.

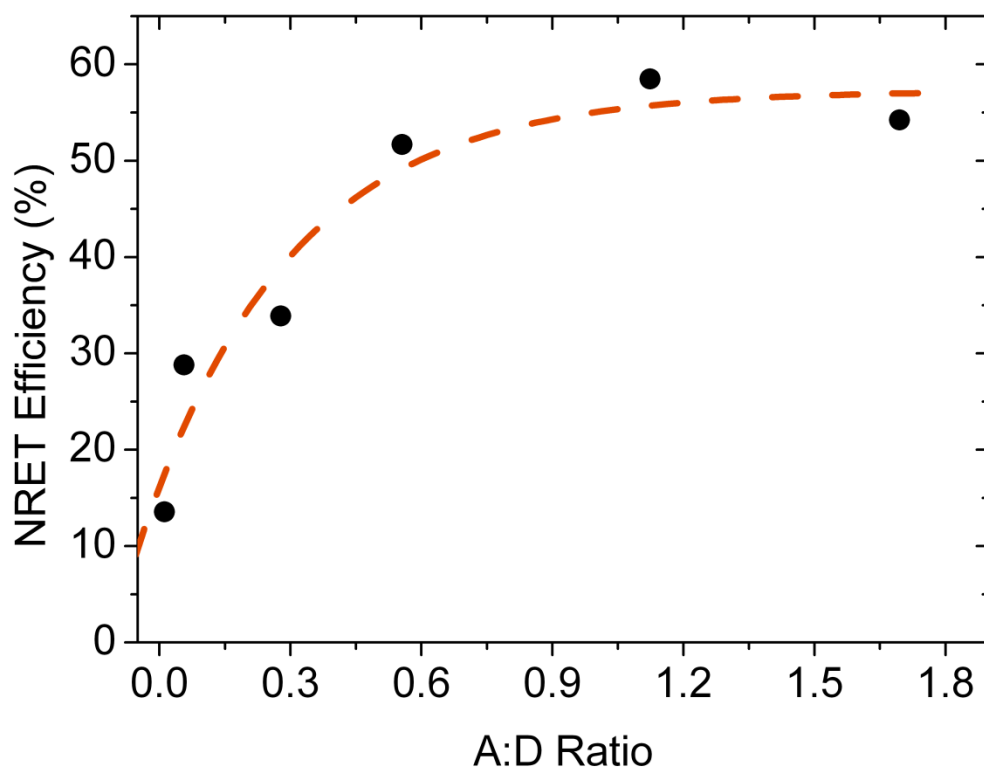


Figure 7. NRET efficiency as a function of A:D ratio.

To understand the possible reason of this limited NRET, we synthesized 5 ML NPLs that intentionally contain ~5% of 4 ML NPLs as a side product of the synthesis (i.e., a mixed NPL solution containing 5 ML NPLs with a population of ~95%). This time we did not perform size selective precipitation such that these mixed NPL populations stay together. Then, we casted the mixed solution on TEM grids to investigate their solid film assemblies via TEM imaging. Here, the 4 ML NPLs have the square-like shape with an average size of 10.81 nm (± 0.53 nm) and the 5 ML NPLs have a rectangle-like shape with an average size of 43.67 nm (± 3.31 nm) and 12.94 nm (± 1.51 nm) (see Figure S1). We observe severe stacking of the NPLs within their own population. Figure 8 demonstrates the HAADF-TEM image of the mixed solid film together with the representative cartoon to illustrate the limitation of the NRET resulting from the nanoscale

phase segregation between the donor and acceptor NPL populations due to their self-stacking. Here NRET is found limited with the longer lateral size of the NPLs, which is on the order of 10 nm, since it is not possible to achieve inter-mixed stacked assemblies of the different populations of NPLs, but instead the mixture of the self-stacked assemblies. Due to this nanoscale phase segregation, NRET efficiencies are limited to ~60% corresponding to almost average separation about the Förster radius (i.e., 10.83 nm), which matches well with the center-to-center separation of 10.61 nm ($0.5 \times 12.17 \text{ nm} + 0.5 \times 9.04 \text{ nm}$) between two adjacent donor and acceptor NPLs. A similar type of phase segregation has been also observed in the conjugated polymer – colloidal quantum dot based hybrids limiting the NRET in those organic–inorganic assemblies.^{23,24} Due to this larger separation between the donor and acceptor species, higher order multi-polar interactions are not expected to be significant.²⁵

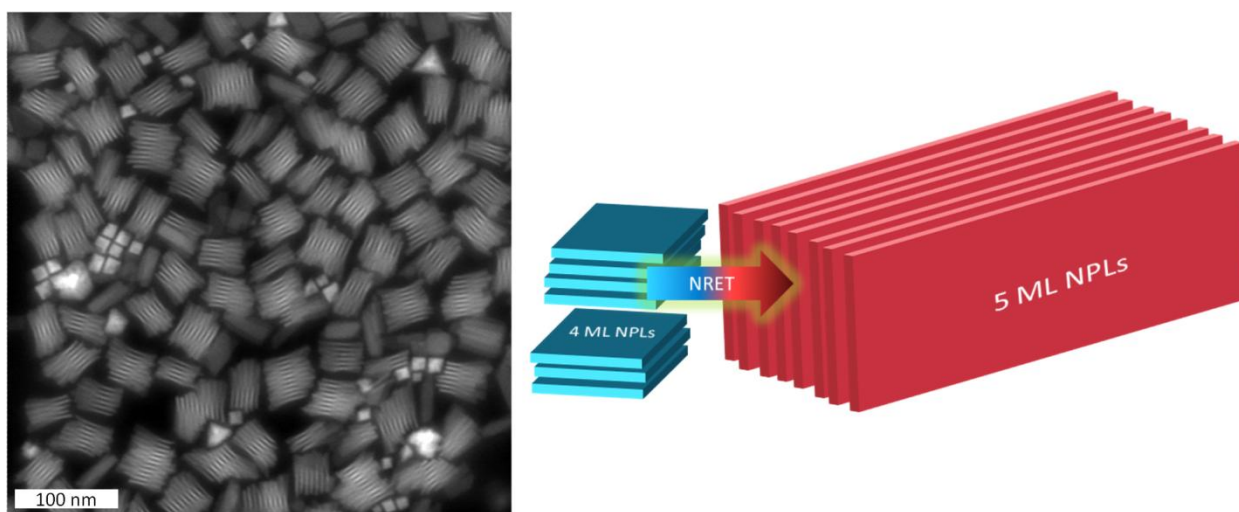


Figure 8. HAADF-TEM image of the mixed NPL assembly (without size selective precipitation) of square-like 4 ML NPLs and rectangle-like 5 ML NPLs. Schematic of the NRET as limited by the nanoscale phase segregation between the NPLs of different populations.

In summary, we have demonstrated the first account of the spectral evidence of the nonradiative energy transfer in the solid thin film assemblies incorporating colloidal CdSe nanoplatelets of different vertical thicknesses. Both steady state and time resolved fluorescence spectroscopy

proves that excitons generated in the donor, 4 ML thick NPLs can be funneled into the acceptor, 5 ML thick NPLs via near field dipole-dipole coupling. The efficiency of NRET can reach 60%, however, further increase in the efficiency is limited by the nanoscale phase segregation between the donor and acceptor NPL populations due to the self-stacking of the NPLs within their own populations leading to increased distance between the donor-acceptor pairs. This type of nanoscale phase separation has not been observed in the mixed solid films of the quantum dots and nanorods to date. As a future work, we are developing inter-stacked NPL assemblies of mixed populations to boost the NRET efficiencies in the assemblies of the NPLs.

EXPERIMENTAL SECTION

Synthesis of the 4 ML NPLs: For a typical synthesis, 170 mg of cadmium myristate, 12 mg of selenium and 15 mL of octadecene (ODE) are loaded into a three-neck flask. After evacuation of the mixed solution at room temperature, it is heated to 240⁰C under inert atmosphere. When the temperature reaches 195⁰C, the color of solution becomes yellowish. Then, 80 mg of cadmium acetate dihydrate is introduced. After 10 mins growth of CdSe NPLs at 240⁰C, the reaction is stopped and cooled down to room temperature with the injection of 0.5 mL of oleic acid (OA). The resulting 4 ML CdSe NPLs are separated by other reaction products with successive purification steps.

Synthesis of the 5 ML NPLs: 170 mg of cadmium myristate and 15 mL of ODE are loaded into a three-neck flask. After evacuation of solution at room temperature, the solution is heated to 250⁰C under inert atmosphere. 12 mg of Se dispersed in 1 ml ODE is swiftly injected. 80 mg of cadmium acetate dihydrate is introduced one minute later. After 10 minutes growth of CdSe NPLs at 250⁰C, the reaction is stopped and cooled down to room temperature with the injection

of 0.5 mL of OA. 5 ML CdSe NPLs are separated by other reaction products with the successive purification steps.

Purification and size-selective precipitation of the nanoplatelets:

As-synthesized NPLs were centrifuged at 4500 rpm for 5 min. The supernatant solution was removed from the centrifuge tube. The precipitate was dried under nitrogen and dissolved in hexane and centrifuged again at 4500 rpm for 10 min. The supernatant was used for the further process. Ethanol was added into the supernatant solution until it became turbid. Then, the turbid solution was centrifuged at 4500 rpm for 10 min. The precipitate was dissolved in hexane and filtered with 0.20 micrometer filter.

Preparation of the solid NPL thin films: The concentration of the 4 and 5 ML NPL solutions is calculated as 7.976×10^{-7} and 4.493×10^{-8} M, respectively. Samples of 4-5 ML NPL solutions having different acceptor-to-donor (A:D) molar ratios, mixed using ultrasonication for 5 min, are prepared. The quartz substrates of 1.5 by 1.5 cm in size are cleaned using piranha solution for 30 min and cleaned with DI-water and dried in an oven at 80 °C for 30 min. The mixed NPL solid thin films are prepared using spin-coating the mixed solutions at 2000 rpm for 1 min.

Steady state and time-resolved optical characterizations:

Steady state photoluminescence spectra and photoluminescence excitation spectra were collected using Cary Eclipse Fluorescence Spectrometer. Photoluminescence quantum yield measurements were performed in solution phase using Rhodamine 6G reference dye. Confocal microscopy images were collected using Zeiss LSM 510. Ar laser line at 458 nm was employed as the excitation source for the confocal imaging. Time-resolved fluorescence decay kinetics were measured using PicoQuant FluoTime 200 that employ PicoHarp 300 time-correlated single

photon counting (TCSPC) unit and a picosecond pump laser at 375 nm. Fluorescence decay curves were fitted by using FluoFit program using multi-exponential decay functions.

ASSOCIATED CONTENT

Supporting Information

TEM images of the stacked NPLs. This material is available free of charge via the internet at <http://pubs.acs.org>.

AUTHOR INFORMATION

Corresponding Author

*volkan@bilkent.edu.tr, hvdemir@ntu.edu.sg

ACKNOWLEDGMENT

The authors would like to thank for the financial support from EU-FP7 Nanophotonics4Energy NoE, and TUBITAK EEEAG 109E002, 109E004, 110E010, 110E217, NRF-RF-2009-09, NRF-CRP-6-2010-02 and A*STAR of Singapore. H.V.D. acknowledges support from ESF-EURYI and TUBA-GEBIP.

REFERENCES

1. S. Ithurria and B. Dubertret, *J. Am. Chem. Soc.*, 2008, **130**, 16504–5.
2. S. Ithurria, M. D. Tessier, B. Mahler, R. P. S. M. Lobo, B. Dubertret, and A. L. Efros, *Nat. Mater.*, 2011, **10**, 936–41.
3. M. D. M. D. Tessier, C. Javaux, I. Maksimovic, V. Lorientte, B. Dubertret, L. T. Kunneman, H. Heuclin, Y. V. Aulin, F. C. Grozema, J. M. Schins, and L. D. A. Siebbeles, *J. Phys. Chem. Lett.*, 2013, **4**, 3574–3578.
4. M. D. Tessier, B. Mahler, B. Nadal, H. Heuclin, S. Pedetti, and B. Dubertret, *Nano Lett.*, 2013, **13**, 3321–8.

5. A. W. Achtstein, A. Schliwa, A. Prudnikau, M. Hardzei, M. V Artemyev, C. Thomsen, and U. Woggon, *Nano Lett.*, 2012, **12**, 3151–7.
6. M. Pelton, S. Ithurria, R. D. Schaller, D. S. Dolzhenkov, and D. V Talapin, *Nano Lett.*, 2012, **12**, 6158–63.
7. Z. Chen, B. Nadal, B. Mahler, H. Aubin, and B. Dubertret, *Adv. Funct. Mater.*, 2014, **24**, 295–302.
8. B. Guzelturk, Y. Kelestemur, M. Olutas, S. Delikanli, and H. V. Demir, *ACS Nano*, 2014, **8**, 6599–6605.
9. C. Bouet, M. D. Tessier, S. Ithurria, B. Mahler, B. Nadal, and B. Dubertret, *Chem. Mater.*, 2013, **25**, 1262–1271.
10. M. D. Tessier, C. Javaux, I. Maksimovic, V. Lorientte, and B. Dubertret, *ACS Nano*, 2012, **6**, 6751–8.
11. M. D. Tessier, L. Biadala, C. Bouet, S. Ithurria, B. Abecassis, and B. Dubertret, *ACS Nano*, 2013, **7**, 3332–40.
12. L. T. Kunneman, M. D. Tessier, H. Heuclin, B. Dubertret, Y. V. Aulin, F. C. Grozema, J. M. Schins, L. D. A. Siebbeles, D. Cdse, C. Cdzn, and C. Shell, *J. Phys. Chem. Lett.*, 2013, **4**, 3574–3578.
13. L. Biadala, F. Liu, M. D. Tessier, D. R. Yakovlev, B. Dubertret, and M. Bayer, *Nano Lett.*, 2014, **14**, 1134–9.
14. T. Förster, *Ann. Phys.*, 1948, **437**, 55–75.
15. B. Guzelturk, P. L. H. Martinez, Q. Zhang, Q. Xiong, H. Sun, X. W. Sun, A. O. Govorov, and H. V. Demir, *Laser Photon. Rev.*, 2014, **8**, 73–93.
16. A. L. Rogach, *Nano Today*, 2011, **6**, 355–365.
17. A. R. Clapp, I. L. Medintz, and H. Mattoussi, *Chemphyschem*, 2006, **7**, 47–57.
18. A. Yeltik, B. Guzelturk, P. L. Hernandez-Martinez, A. O. Govorov, and H. V. Demir, *ACS Nano*, 2013, **7**, 10492–501.
19. B. Abécassis, M. D. Tessier, P. Davidson, and B. Dubertret, *Nano Lett.*, 2014, **14**, 710–5.
20. C. She, I. Fedin, D. S. Dolzhenkov, A. Demortière, R. D. Schaller, M. Pelton, D. V Talapin, and D. Richard, *Nano Lett.*, 2014, **14**, 2772–7.
21. C. Kagan, C. Murray, M. Nirmal, and M. Bawendi, *Phys. Rev. Lett.*, 1996, **76**, 1517–1520.

22. J. R. Lakowicz, *Principles of Fluorescence Spectroscopy*, Springer US, Boston, MA, 2006, vol. 13.
23. T. Stoferle, U. Scherf, and R. F. Mahrt, *Nano Lett.*, 2009, **9**, 453–456.
24. B. Guzelturk, P. L. Hernandez Martinez, V. K. Sharma, Y. Coskun, V. Ibrahimova, D. Tuncel, A. Govorov, X. Sun, Q. Xiong, and H. V. Demir, *Nanoscale*, 2014.
25. T. W. J. Gadella, *Fret and Flim Techniques*, Elsevier, 2009, vol. 33.